Survey of Multi-Scale Meshfree Particle Methods

Lucy T. Zhang[1], Wing K. Liu[1], Shao F. Li[2], Dong Qian[1], and Su Hao[1]

[1] Northwestern University, Evanston IL, USA.
[2] University of California, Berkeley CA, USA.

Abstract. A multiscale meshfree particle method is developed, which includes recent advances in SPH and other meshfree research efforts. Key features will include linear consistency, stability, and both local and global conservation properties. In addition, through the incorporation of Reproducing Kernal Particle Method(RKPM), standard moving least squares (MLS) enhancement and wavelet techniques, the method have the flexibility of resolving multiple scales in the solution of complex, multiple physics processes. We present the application of this approach to the following areas: 1) simulations on propagation of dynamic fracture and shear band; 2) impact and penetration; 3) fluid dynamics and 4) nano-mechanics.

1 Introduction

Meshfree methods are a new class of methods that offer the potential to treat difficult multi-scale problems, including problems of material failure, fracture, and fragmentation. Since failure and fracture processes are associated with damage evolution, it is important to choose the correct computational multiphysics material models. Generally, damage evolution and failure start from one or more local regions in a material, wherein a crack growth begins due to localized damage, thereby leading to damage concentrations that finally result in material fracture. Modeling the failure process can be idealized by studying the discrete energy transfer from the larger scales to the smaller scales. Meshfree methods can deal with the multi-scale phenomena inherent in failure of materials more naturally than finite elements, thus providing an added impetus to simulating these problems with realistic physical models. We expect that each scale can reproduce a particular physical phenomenon such as nucleation, high amplitude strain and damage concentration, or movement of dislocations. Therefore, major goals are to advance multi-scale meshfree methods for the modeling of material failure, and to link the micro-scale notion of dislocations, the meso-scale plastic strains and strain gradient, and the macro-scale continuum mechanics within a multi-scale framework. To the authors' knowledge, current simulation methods do not have multi-scale capabilities.

Methodologies can be developed for treating problems involving widely varying scales, such as shear band formation and localized deformations, which are important in the prediction of failure. To meet the demands of

modern software, error estimators, hp adaptivity, multiresolution analysis, sampling approximations, and edge detection, among others should be developed. The proposed approach is fundamentally different from the traditional finite element methods. It could play a significant role in the next generation of discretization methods for fracture and fragmentation in proof-test simulations. The main reasons to promote this speculation, in our opinion, are twofold: the methods' ability to abandon the mesh generation and their flexibility to embed multi-physics of the specific problem into the interpolation function basis.

2 The multiscale meshfree particle method

Despite its success in the analysis of geometric and material nonlinear behavior in structures and solids, the widely used finite element methods exhibit a number of shortcomings in handling problems involving large deformation, high gradients, or moving discontinuities such as cracks, fracture, fragmentation and multi-scale analysis. Recently, a new generation of numerical methods called "meshfree" methods has emerged and is now profoundly influencing almost every branch of engineering and the physical science. One of the most distinguished features about meshfree methods is that no explicit mesh is needed in the formulation.

As one part of this family, the Reproducing Kernel Particle Method originally evolved from wavelet theory and SPH method. It has been applied successfully to a broad range of problems. In addition to SPH and wavelet theory, meshfree methods modifie the kernel function by introducing a correction function in order to enhance its accuracy near or on the boundary of the problem domain. Due to this correction function suggested by Liu, et al. (1995), the consistency condition is satisfied. Liu, et al. (1995) demonstrated the application of meshfree methods to structural dynamics, and the method was used successfully for large deformation simulations (Chen, et al. 1996, Liu, et al. 1996, Jun, et al. 1998, Liu, et al. 1998), computational fluid dynamics (Liu, et al. 1995). Through the flexibility of choices of window function and dilation parameter, meshfree methods can be used extensively in error estimation, image processing, edge detection and hp-adaptivity algorithms.

Multiple scale method can be an effective method for simulating failure processes. These failure processes are encountered in the interactions between many different length scales. For instance, these interactions can be seen between bond length which are in the order of an Angstrom, dislocations which are associated the scales from nanometers to microns and shear bands which are of the order from microns to macroscopic size. In the failure analysis, the challenges are discovering the features of interactions at different length scale and the behaviors that are dependent of the scales.

The multiscale simulation method will be developed based on the new techniques for coupling between disparate length scales. Two approaches are

proposed for the multiscale modelings: hierarchical multiscale and concurrent multiscale modelings. The hierarchical is a method to embed defects such as dislocations and quantum calculations in the continuum model by using the enrichment solutions and the multi-physics material models. This method also allows the use of data from quantum mechanics (QM), molecular dynamics (MD) or continuum mechanics (CM), as well as analytical and experimental results to provide information for and to be coupled with coarse scale computations in efficient multiscale simulations. It is a new computational tool that links scales from quantum mechanics to continua. This dynamically coupled QM/MD/CM method is used for the applications from selected engineering systems. The concurrent multiscale modeling enables the low scale solution representation to co-exist with the discrete atomic representation in a given region. The coupling between them is handled by the bridging scale method.

Parallel and distributing computation will be used on the tera-scale machines for the multi-scale simulation methods that are to be developed. A scalable and suitable parallelization algorithm or methodology will be developed to minimize load imbalance and communications. These parallel multiscale simulations will be developed based on the existing continuum, molecular and quantum mechanics codes.

This simulation of the integrated environment of failure at continuum, micro- and atomic scales will provide understandings of multi-physics of the integrated engineering system and the interplays between dynamics at a wide range of scales. The methods will be applied to the study of fracture and shear band so that the behavior of failure can be better understood at various length scales. The fracture will first be studied in the simplest non-trivial yet tractable system. We will then consider more complex systems such as fracture at polymer/ceramic interfaces and shear banding.

3 Simulation on propagation of dynamic fracture and shear band

In 1996, Zhou, Rosakis et al. (1996a) performed a set of experiments in which a high-speed cylindrical projectile impacted a pre-notched rectangular plate. Their major finding was that as the impact velocity increased, the mode of failure went from brittle (crack propagation) to ductile (dynamic shear band propagation), which contradicts the traditional school of thought. Others have conducted similar experiments, notably Mason et al (1994), Kalthoff and Winkler (1987), and Ravi-Chandar (1995).

The numerical simulations of the Zhou experiment have had mixed results. Some researchers, such as Zhou, Rosakis et al. (1996b) have been able to predict the dynamic shear band propagation, while others, notably Klein (1999) and Belytschko et al (1996) have been able to capture the correct crack initiation angle. The numerical results of Zhou and others have suffered

from mesh dependence. Although both studies predict shear band propagation, the shear band is constrained to propagate in a straight line along the element boundaries. In contrast, experimental results show that the shear band actually propagates in a curved direction, and that the curvature is a function of the impact speed. Thus the ability to capture both the failure mode/transition and the dynamic shear band propagation remained an open problem.

These shortcomings motivated researchers at Northwestern to further analyze the Zhou and Rosakis experiment. Using RKPM, a meshfree numerical method, Li and Liu (2000,2001), ([12],[13]) were able to predict for the first time:

- The ductile-to-brittle failure mode transition observed that is observed experimentally
- A curved shear band whose character changes as a function of the projectile impact speed (see Fig. 1)
- A periodic temperature profile matching that obtained experimentally (Rosakis, 2000)
- An intense, high strain rate region in front of the shear band tip, which we believe to cause a stress collapse that drives the formation and propagation of a dynamic shear band (see Fig. 3)

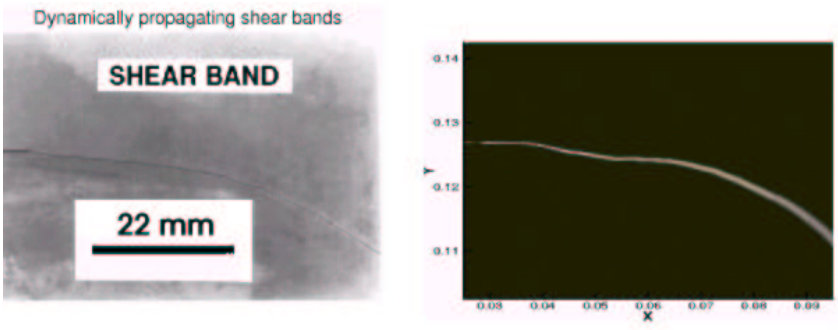

Fig. 1. Comparison of experimental result with computation. Results are taken from [12].

A phenomenon called "temperature reflection" that can only be seen in 3D calculations. In this phenomenon, the temperature at the end of the plate has already risen before the shear band tip has reached that region, which is similar to the spalling phenomenon of a target/projectile problem.

Multiple-scale decomposition and analysis of the shear band. In analyzing the shear band at different scales, one can first observe the macroscopic

prediction of the curved shear band. Then by magnifying the shear band, one can gradually resolve the detail of the shear band to the point where the periodic temperature profile of the shear band can clearly be seen. (see Fig. 2)

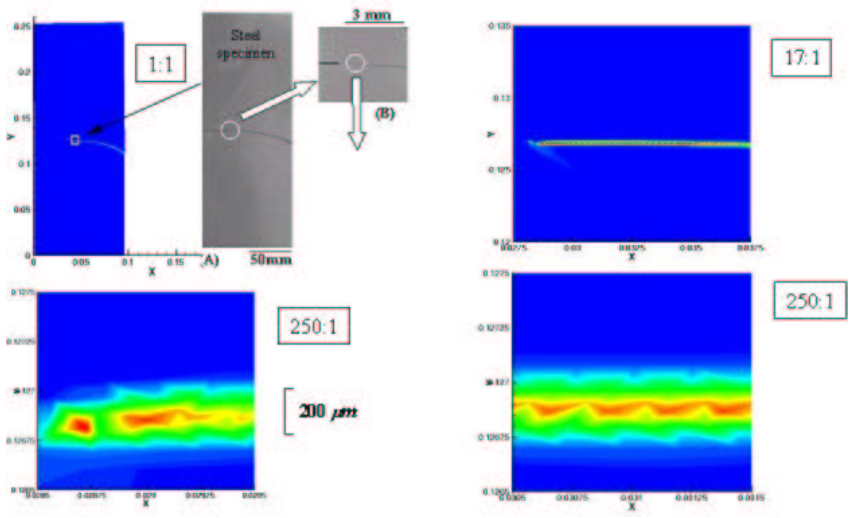

Fig. 2. Multiple scale analysis of shear band temperature field. Results are taken from [12].

Preliminary results related to dynamic shear band propagation can be found at: http://www.tam.nwu.edu/wkl/liu.html

In most computer simulations of strain localization, shear band formation is the outcome of a bifurcated solution sought in numerical computations due to material instability. However, how to simulate the propagation of such material instability is still an open problem, and the earlier numerical simulations fail in simulating the propagation of shear band formation. The key technical ingredient in such simulations, we believe, is how to simulate the collapsing state of shear band formation. And it is found that the stress collapse in the newly formed localization zone (shear band tip) promotes or triggers the shear band's further propagating. To simulate stress collapse state inside the shear band, a so-called shear band damage model is introduced, which conforms to physicists' belief that instead of being a bifurcated mathematical solution a shear band is a physical entity, within which there is significant weakening, or changes in material properties which may even be identified as phase transformation. In order to simulate the collapsing state of shear band formation, a thermal-viscous Newtonian fluid damage model

was adopted by Li and Liu (2001), ([12], [13]), similar to that proposed by Zhou et al (1996a). The choice of such a multi-physics model is necessitated by the many mechanisms that drive the formation and propagation of a shear band.

In addition, there are also many new physics revealed from this simulation. The distribution of the strain rate and a detail look at the structure are shown in Fig 3. From the numerical results, we found that a self-similar strain rate field moves with the propagation of the shear band tip, this is quite similar to the self-similar singular stress field moving in front of a crack tip. We propose that the concentrated strain rate field in front of the shear band tip might be the driving force for the formation of shear band under high-speed impact. Therefore, a close link between the strain rate field concentration and stress collapse must be established in the proposed modeling.

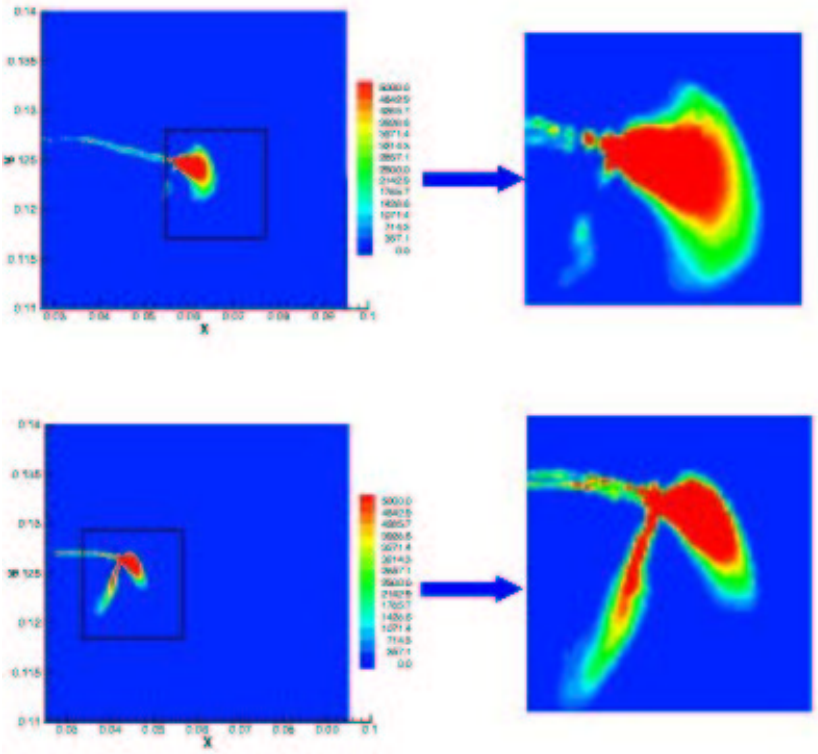

Fig. 3. Strain rate contour and detail structure at 36 μs (top) and 48 μs (bottom) (impact speed v=37m/s). Note the appearance of a stress collapse zone at the shear band front. Results are taken from [12].

4 Impact and penetration problems

A dynamic, explicit, large deformation version of meshfree particle method has been also developed for three dimensions. To test it in a real world engineering application, it has been applied to a high-speed penetration simulation. The computation has been compared with experimental data obtained by the Army Water Station. The problem statement is given in Fig 4. Two cases have been studied: a single projectile case and a multiple projectile case. In both cases the projectile has an initial velocity more than Mach 5. The target is made of rebar reinforced concrete. A multi-scale damage constitutive law is used in the simulation. Figures in 5 show damage contours for the single and multiple penetrator cases, respectively. Fig 6 shows the result of the computed penetrator depth compared with the experimental data. Note in 5 that the particles that have been displaced by the penetrator have been squashed, representing the degree of damage in the material element lumped at these particles. The mass of the material is thus preserved, and no artificial erosion algorithm is necessary. The complete MPFEM 3D large deformation formulation will be provided in the subsequent paper (Hao et.al.2001).

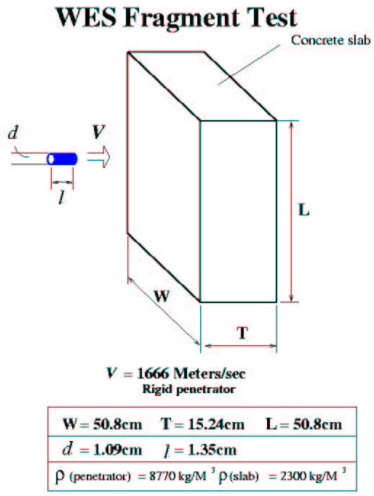

Fig. 4. Problem statement for penetration simulation. Problem is taken from [6].

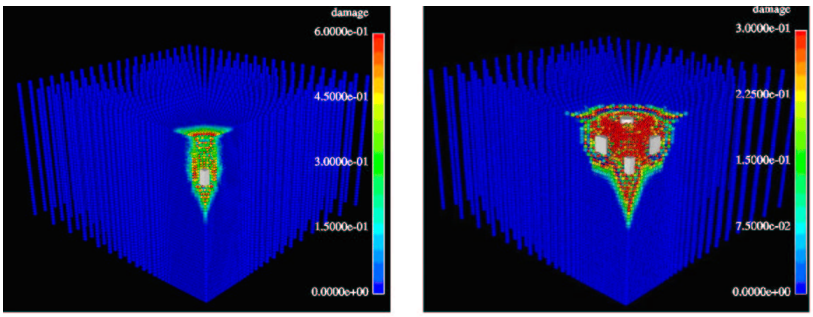

Fig. 5. Damage contours for single and multiple penetrator case. Results are taken from [6].

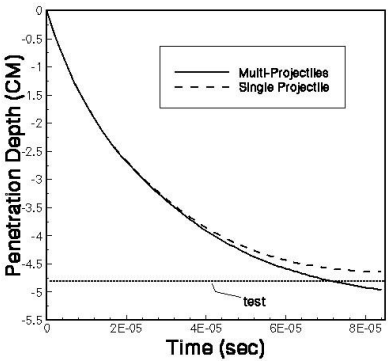

Fig. 6. Comparison of MPFEM simulation to experimental result. Results are taken from [7].

5 Fluid dynamics

A parallel computational implementation of the Reproducing Kernel Particle Method (RKPM) is used for 3-D implicit CFD analysis. Even though meshfree methods involve more computation time due to the shape functions, parallelization scheme enables us to solve large size problems in a reasonable amount of time. A uniform flow past a cylinder is simulated as an example problem. A cylinder with a diameter of 1.5cm with its axis in the z-direction is placed in a uniform x-directional flow. The dimensions of the computational domain is $21.5cm \times 14cm \times 4cm$, and the cylinder is located 4.5cm downstream of the inflow as shown in Fig. 7. A more detailed description can be found in [30].

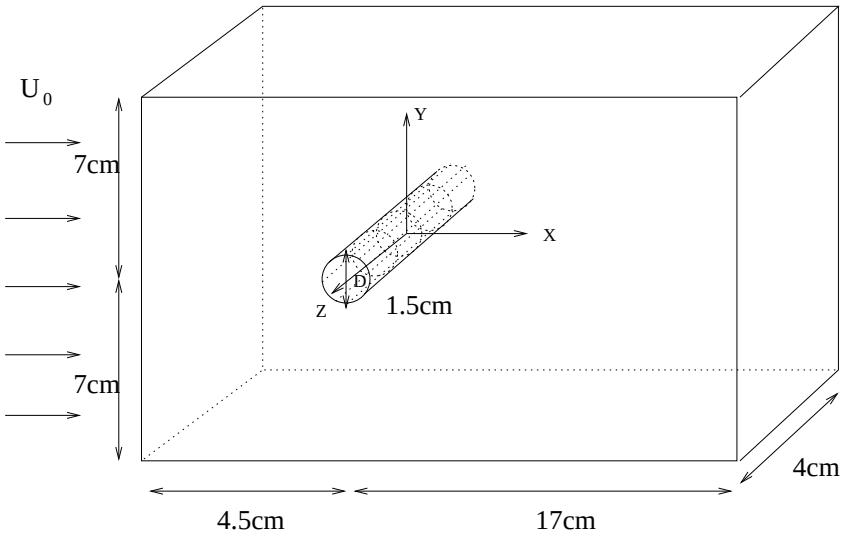

Fig. 7. Flow past a cylinder. Problem is taken from [30].

Two different discretizations are used: a coarse discretization with 2236 nodes and 11628 integration points, and a fine discretization with 15447 nodes and 87646 integration points. For both nodal distributions, the discretization is finest near the cylinder surface in order to resolve the boundary layer. Initially, the velocity is uniform with speed U_0 everywhere. For $t > 0$, $\mathbf{u} = \mathbf{0}$ is enforced on the surface of the cylinder. The inflow boundary condition at $x = -4.5cm$ is uniform flow of speed U_0, while the outflow at $x = 17cm$ is a zero-stress boundary. The top, bottom, and sides of the computational domain have zero penetration conditions, but allow slip parallel to the walls. The time $T = U_0 t/a$ is non-dimensionalized based on the uniform velocity

U_0 and the radius of the cylinder, a. The 3-D streamline contours of the flow field for Reynolds numbers of 200 and 1000 at different times are presented in Fig. 8. The vortices and their developments through the early times can be clearly seen in the figures. The boundary is treated using the hierichical bridging enrichment method (EBC). The drag coefficients are plotted against different Reynolds Numbers that range from 10 to 1000 and are compared with the values obtained from experiments, FEM and RKPM without enrichment in Fig. 9. In the algorithm of RKPM without enrichment, the essential

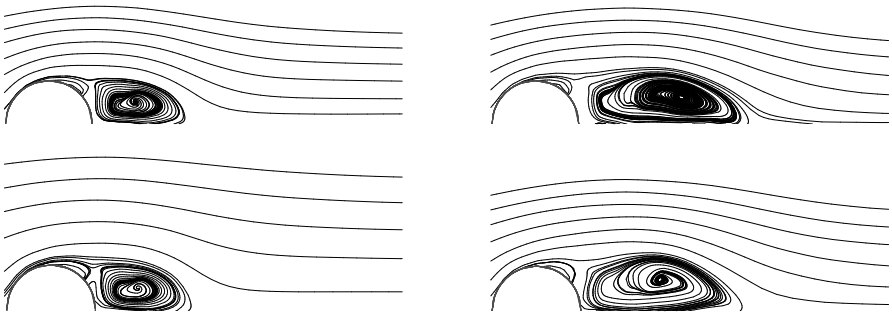

Fig. 8. Streamlines for Re=200 and Re=1000 at T=5 and T=10 using RKPM. (**a**) Re=200, T=5 (**b**) Re=200, T=10 (**c**) Re=1000, T=5 (**d**) Re=1000, T=10. Results are taken from [30].

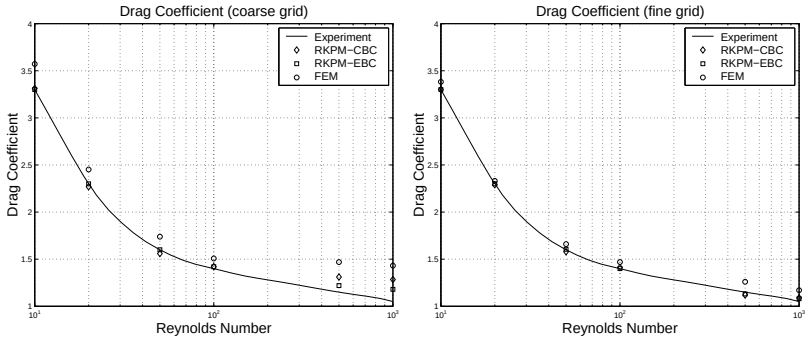

Fig. 9. Drag coefficient of the cylinder vs. Reynolds number. CBC: Collocation Boundary Condition implementation; EBC: Enrichment Boundary Condition (**a**) coarse grid (**b**) fine grid. Results are taken from [30].

boundary is treated using the "corrected collocation" method (CBC). As shown on the plot, using the enrichment method to implement the essential boundary yields results closer to the experimental values than the one without, but both methods are more accurate than FEM. Our results indicate that even the coarse discretization is sufficiently fine to obtain accurate results using RKPM, while the FEM solution is not fully resolved even with the fine mesh. The parallel performance on the Cray T3E for this problem is shown in Fig. 10. The speedup is scaled based on the calculation time of 4 processors. Although the calculation performance can not reach the ideal case of linear speedup, we are still be able to see the speedup when running the fixed-size problem using up to 32 processors. Communication then dominates the running time as the number of processors is increased to 64.

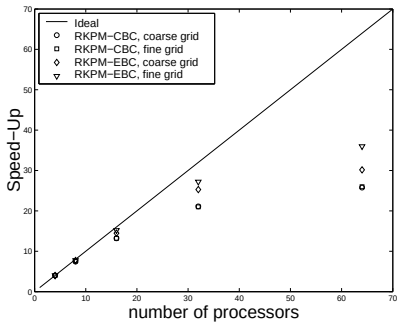

Fig. 10. Parallel performance on CrayT3E of RKPM for flow past a cylinder problem (speedup is calculated based on the calculation time of using 4 processors). CBC: Collocation Boundary Condition implementation; EBC: Enrichment Boundary Condition implementation. Results are taken from [30].

6 Computational nanomechanics

Materials at the nanoscale have demonstrated impressive physical, electrical and chemical properties, thus suggesting a wide range of areas for application. For instance, carbon nanotubes are projected to be remarkably stiff and strong and conduct electricity and heat better than copper at room temperature, suggesting their eventual role in light weight, high-strength materials such as cabling and discontinuous fiber reinforced composites, and as both devices and nanowires in molecular electronics. They are under intensive study as an efficient storage medium for systems ranging from alkali ions for nanoscale power sources to hydrogen for fuel cells. Future possible application of nanotubes includes as accurate drug delivery systems.

The existence of fullerenes inside nanotubes has been observed as a product of different processes of synthesizing nanotubes. For instance, Smith et al (1998) used pulsed laser evaporation (PLV) of a catalyst-containing graphite target, Sloan et al (2000) and also Zhang et al (1999) who used arc vaporization of carbon with a mixed Ni/Y catalyst. Thus fullerenes inside of nanotubes is an experimental reality from work in the last few years, and there has been no reported modeling of these structures in the literature to our knowledge. One may speculate that fullerenes encapsulated inside of nanotubes could significantly affect the physical properties relative to the empty nanotube. Questions naturally arise about the geometries that the hybrid NT/fullerene systems adopt, the resulting elastic properties and energetics, and about certain issues related to the tribology of the system. In addition to achieving fundamental understanding, it is interesting to study such peapod structure as potential functional devices e.g., as nano-pistons, nano-bearing systems, nano-writing devices, or nano-capsule.

A modeling study of nanotubes filled with fullerenes is presented, with focus on a new approach. The objective is to investigate the mechanics of this nanotube/fullerene system, such as the elastic properties, energetics, and certain tribological issues. We have proposed a combined molecular dynamics /continuum approach with account of both the non-bonded and bonded interactions. The derived elastic properties from the Tersoff-Brenner potential are consistent with experimental observations.

In the simulation, we choose the lengths of all the nanotubes to be L = 129 $\boldsymbol{r}A$. The nanotubes are modeled as a cylindrical shell with thickness t. The value of t is corresponding to the interlayer distance of graphite sheet or equivalently, the Van der Waal force distance. The C_{60} is modeled directly using the Tersoff-Brenner potential. The computation is performed in a scaled system with the following ratios (superscript * denotes the scaled system): Mass Density $\rho^*/\rho = 1$, Young's Modulus $E^*/E = 1$, Length $L^*/L = 10^{10}$, Time $t^*/t = 10^{10}$, Energy $U^*/U = 10^{30}$, Mass $m^*/m = 10^{30}$.

The time step in the scaled system is chosen as $dt^* = 5 \times 10^{-5}$, this corresponds to 5×10^{-15} *sec*. The Verlet integration scheme has been adopted for both the continuum (the nanotube) and the molecular (C_{60}) system. The configurations are saved every 0.5 *ps*. The system is first cooled to 0 K using a relaxation scheme. All the computations are performed on a PC with linux operating system. The following cases have been computed:

1) C_{60} initially at rest outside, and 10 $\mathring{A}$ away on-axis, from the open end of a (10,10) nanotube.

2) Same as 1), but with a (9,9) nanotube.

3) C_{60} is initially at the same position as 1) and 2), but is fired with a finite initial velocity, on-axis towards the open ends of the (5,5), (6,6), (7,7), and (8,8) nanotubes, respectively.

Case (1) was first computed for a total time of 200 *ps* and 500 *ps*, respectively. Shown in Fig.11a is the binding energy as a function of the accumulated displacement of C_{60}. A low energy plateau is reached after 10 *ps*.

Simulation indicates that without any external action, C_{60} was sucked into the tube from the open end. Fig.11b shows the corresponding total force components, with f_z the axial component of force. The C_{60} does not escape from the (10,10) tube, but rather is decelerated at the opposing end due to a strong restoring force. While inside the tube, the axial component of force is smaller than the force in the radial directions. The same conclusion can be inferred from Fig.11d, in which an almost constant level of speed along the axial direction is observed. It is interesting to see that the C_{60} oscillates along the axis inside the nanotube, going back and forth between the two open ends, and never escaping. Moreover, the magnitude of the oscillation, after a few cycles (Fig.11e), is almost constant and shows no sign of decay. The period of the oscillation can be estimated from the generated data, which is between 47.38 to 64.10 ps for a (10, 10) nanotube with length of 129 $\mathring{A}$. In addition, the forces in the x and y directions start to grow (Fig.11c) after the C_{60} is sucked back in from the opposing end. The average radius of the C_{60} was computed for each saved configuration (obtained every 0.5 ps as mentioned above). This computed average radius was always within ± 0.02 $\mathring{A}$ of the radius of an undeformed C_{60}. On the other hand, the average radius of the (10,10) tube (obtained every 0.5 ps) was found to be within ± 0.15 $\mathring{A}$ of the undeformed tube radius. The (10,10) tube is observed to have moderate temperature increase (< 1.8 K).

We now consider the interaction between C_{60} and the (9,9) nanotube. In this case the C_{60} is still sucked into the tube when initially at rest. However, the radial deformation of the tube and its interaction with the C_{60} are stronger than in (10, 10), and both the binding energy and radial force components oscillate strongly. The axial component of force is larger than for the (10, 10) nanotube, and the average axial velocity is lower. The spread in C_{60} radius values is ± 0.025 $\mathring{A}$, which is slightly higher than for the C_{60} in the (10,10) tube. The (9,9) tube radius changes are similar to that for the (10,10) tube case.

For case 3, we applied an initial velocity from 400 to 1600 m/sec on the C_{60} in the axial direction to see if it would enter the (8,8), (7,7), (6,6) and (5,5) tubes. For all these cases the C_{60} is not able to enter due to the strong repulsive action. the open tip. For a detailed description, the animations are available on the web (http://tam.nwu.edu/wkl/c60_in_tube).

The analysis of the interaction between the fullerene C_{60} and 5 different armchair nanotubes is done by a combined continuum/molecular dynamics approach. This approach bridges the bonding potential with the continuum property of the material, which additionally serves as a useful tool for evaluating the bonding potentials. An interesting phenomenon is observed from the simulation in which C_{60} is 'sucked' into the (10, 10) or (9,9) tube by the sharp surface tension force present in the front of the open end and then oscillates between the two open ends of the nanotube, never escaping. Moreover, the oscillation shows little decay after stabilizing after a few cycles. Both the C_{60} molecule and the nanotube show small deformations as a function of time

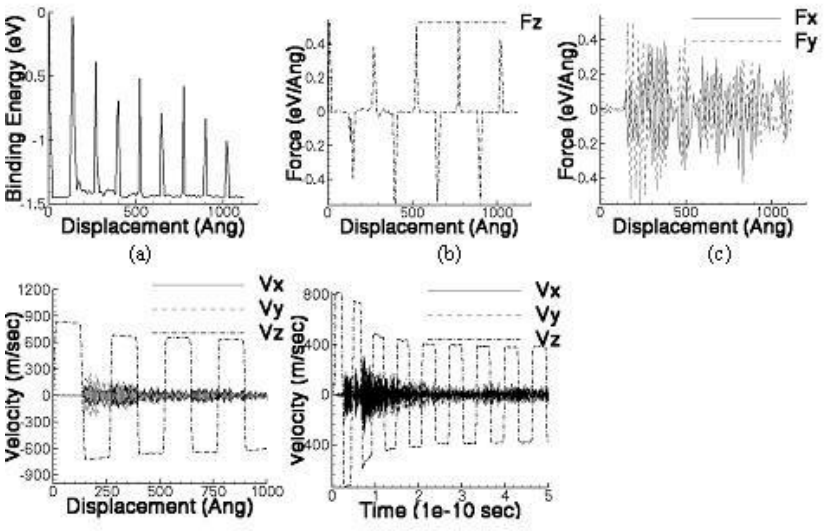

Fig. 11. (**a**) Binding energy as a function of displacement for C_{60} traversing the (10,10) nanotube eight times (back and forth, thus 4 full cycles). (**b**) The total axial force acting on the C_{60}. (**c**) The x and y component of the total force acting on the C_{60}. (**d**) The three velocity components of the C_{60}. (**e**) The three velocity components history of the C_{60} as it traverses the (10,10) nanotube twenty times. Results are taken from [22].

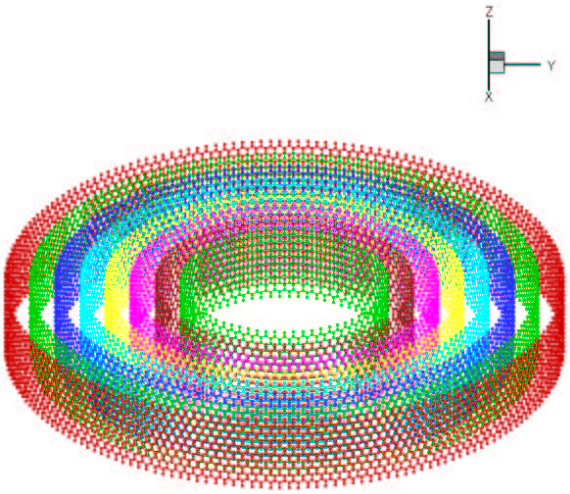

Fig. 12. Multi-walled Carbon Nanotube.

and position. Furthermore, C_{60}, even when fired on axis with an initial speed up to 1600m/sec, cannot penetrate into any of the (8,8), (7,7), (6,6) and (5,5) nanotubes. The simulation results suggest the possibility of use of C_{60} in nanotubes for making nano-devices such as a nanobearing or nano-piston.

The analysis of the multi-walled carbon nanotubes is currently under investigaton. The model is shown in Fig. 12. The mechanical and electrical properties of these multi-walled nanotubes will provide useful results that benefit the related on-going experiments.

7 Conclusions

The following goals have been achieved:

- A wavelet-based meshfree particle method is developed to form the foundation of multi-scale analysis.
- Methodology for linking micro-scale dislocations to the meso-scale damage models in multi-scale multi-physics methods is developed.
- Enrichment methods based on length scale dependent theories have been incorporated into the proposed computational models.
- Computational multi-physics methods will be developed to improve the predictions made for strain-softening behavior that generally coincide with most damage analyses.
- Approaches to efficiently distribute computations onto large numbers of parallel processors will be concurrently developed with the foregoing meshfree methods.
- A meshfree continuum approach for the analysis of nano-scale system has been proposed and successfully implemented.
- A combined molecular dynamics/continuum approach with account of both the non-bonded and bonded interactions.

Acknowledgment. This work is supported by the grants from National Science Foundation, the Army Research Office, and Tull Family Endowment.

References

1. M. Bar-Lev and H.T. Yang. Initial flow field over an impulsively started circular cylinder. *Journal of Fluid Mechanics*, 72:625–647, 1975.
2. T. Belytschko and T. Tabbara. Dynamic fracture using efg. *IJNME*, 39:3, 1996.
3. J.S. Chen, C. Pan, C.T. Wu, and W.K. Liu. Reproducing kernel particle methods for large deformation analysis of nonlinear structures. *Computer Methods in Applied Mechanics and Engineering*, 139:195–227, 1996.
4. W.M. Collins and S.C.R. Dennis. The initial flow past an impulsively started circular cylinder. *Quarterly Journal of Mechanics and Applied Mathematics*, 26:53–75, 1973a.
5. W.M. Collins and S.C.R. Dennis. Flow past an impulsively started circular cylinder. *Journal of Fluid Mechanics*, 60:105–127, 1973b.

6. S. Hao, W.K. Liu, P. Klein, and D. Qian. Multi-scale damage model. *manuscript to be submitted*, 2001.
7. S. Hao, H. Park, and W.K. Liu. Moving particle finite element method. *submitted*, 2001.
8. S. Jun, W.K. Liu, and T. Belytschko. Explicit reproducing kernel particle methods for large deformation problems. *International Journal for Numerical Methods in Engineering*, 41:137–166, 1998.
9. J.F. Kalthoff and S. Winkler. Failure mode transition at high rates of shear loading. *C.Y. Chiem, H.D. Kunze and L. W. Meyer, edts., Impact Loading and Dynamic Behavior of Materials*, 1:185–195, 1987a.
10. P.A. Klein. *Technical Report*. Sandia National Laboratories, 1999.
11. S. Li and W.K. Liu. Meshfree and particle methods and their applications. *accepted for publication in Applied Mechanics Review*, 2001.
12. S. Li, W.K. Liu, D. Qian, P. Guduru, and R. Rosakis. Dynamic shear band propogation and micro-structure of adiabatic shear band. *Comp. Meth. In Applied Mech. Engrg*, in press, 2001.
13. S. Li, W.K. Liu, A. Rosakis, T. Belytschko, and W. Hao. Meshfree galerkin simulations of dynamic shear band propagation and failure mode transition. *accepted for publication in Journal of Mechanics and Physics of Solids*, 2000.
14. W.K. Liu and Y. Chen. Wavelet and multiple scale reproducing kernel methods. *International Journal for Numerical Methods in Engineering*, 21:901–931, 1995.
15. W.K. Liu, Y. Chen, R.A. Uras, and C.T. Chang. Generalized multiple scale reproducing kernel particle methods. *Computer Methods in Applied Mechanics and Engineering*, 139:91–158, 1996.
16. W.K. Liu and S. Jun. Multiple scale reproducing kernel particle methods for large deformation problems. *International Journal for Numerical Methods in Engineering*, 41:1339–1362, 1998.
17. W.K. Liu, S. Jun, J. Adee, and T. Belytschko. Reproducing kernel particle methods for structural dynamics. *International Journal for Numerical Methods in Engineering*, 38:1655–1680, 1995.
18. W.K. Liu, S. Jun, D.T. Sihling, Y. Chen, and W. Hao. Multiresolution reproducing kernel particle method for computational fluid dynamics. *International Journal of Numerical Method in Fluids*, 24:1391–1415, 1997.
19. W.K. Liu, S. Jun, and Y.F. Zhang. Reproducing kernel particle methods. *International Journal for Numerical Methods in Engineering*, 20:1081–1106, 1995.
20. W.K. Liu, R.A. Uras, and Y.Chen. Enrichment of the finite element method with the reproducing kernel particle method. *Journal of Applied Mechanics, ASME*, 64:861–870, 1997.
21. J.J. Mason, A.J. Rosakis, and G. Ravinchandran. Full field measurement of the dynamic deformation field around a growing adiabatic shear band at the tip of a dynamically loaded crack or notch. *Journal of Mechanics and Physics of Solids*, 42:1679–1697, 1994.
22. D. Qian, W.K. Liu, and R.S. Ruoff. Mechanics of nanotubes filled with fullerenes. *accepted for publication in Journal of Physical Chemistry B*, 2001.
23. K. Ravi-Chandar. On the failure mode transition in polycarbonate dynamic mixed-mode loading. *International Journal of Solids and Structures*, 32:925–938, 1995.
24. A.J. Rosakis. Private communication. 2000.

25. J. Sloan, R.E. Dunin-Borkowski, J.L. Hutchinson, K.S. Coleman, V.C. Williams, J.B. Claridge, A.P.E. York, C. Xu, S.R. Bailey, G. Brown, S. Fridrichs, and M.L.H. Green. The size distribution, imaging and obstructing properties of c60 and higher fullerenes formed within arc-growth single walled carbon nanotubes. *Chemical Physics Letters*, 316:191–198, 2000.
26. B.W. Smith, M. Monthoux, and D.E. Luzzi. Encapsulated c60 in carbon nanotubes. *Nature*, 336:323, 1998.
27. G. J. Wagner and W.K. Liu. Application of essential boundary conditions in mesh-free methods: a corrected collocation method. *International Journal for Numerical Methods in Engineering*, 47:1367–1379, 2000.
28. G.J. Wagner and W.K. Liu. Hierachical enrichment for bridging scales and meshfree boundary conditions. *International Journal for Numerical Methods in Engineering*, 50:507–524, 2000.
29. M.F. Yu, M.J. Dyer, D. Qian, W.K. Liu, and R.S. Ruoff. Locked twist in multiwalled carbon nanotube ribbons. *accepted for publication in Physical Review B, Rapid Communications*, 2001.
30. L.T. Zhang, G.J. Wagner, and W.K. Liu. A parallelized meshfree method with boundary enrichment for large-scale cfd. *submitted to Journal of Computational Physics*, 2000.
31. Y. Zhang, S. Iijima, Z. Shi, and Z. Gu. Defects in arc-discharg-produced single-walled carbon nanotubes. *Philosophical Magazine Letters*, 79:473–479, 1999.
32. M. Zhou, A.J. Rosakis, and G. Ravichandran. Dynamically propagating shear bands in impact-loaded prenotched plates -i, experimental investigations of temperature signatures and propagation speed. *Journal of Mechanics of Physics and Solids*, 44:981–1006, 1996a.
33. M. Zhou, A.J. Rosakis, and G. Ravichandran. Dynamically propagating shear bands in impact-loaded prenotched plates -ii, numerical simulations. *Journal of Mechanics of Physics and Solids*, 44:1007–1032, 1996b.